# Molecular Plasmonics: Chromophore–Plasmon Coupling and Single-Particle Nanosensors

Jing Zhao, Leif J. Sherry, George C. Schatz, and Richard P. Van Duyne

*(Invited Paper)*

***Abstract*—This review describes investigations into the localized surface plasmon resonance (LSPR) of silver nanoparticles from both experimental and theoretical perspectives. It is divided into two parts: 1) LSPR of silver nanoparticle arrays and its interaction with resonant adsorbates and 2) single-nanoparticle LSPR spectroscopy and sensing of two specific nanoparticle geometries: triangular nanoprisms and nanocubes. Part I addresses the problem of strong coupling between the plasmon resonance of the nanoparticle and the molecular electronic resonances of the adsorbates. In particular, it was shown that the shift in the LSPR wavelength induced by resonant adsorbates binding to nanoparticles is highly dependent upon the relative spectral position of the LSPR to the molecular resonance. This finding was applied to study the electronic structures of resonant adsorbates on metallic nanostructures. Furthermore, an optical nanosensor was designed to study low molecular weight substrate molecule interaction with cytochrome P450 proteins. Part II shows that the LSPR spectra of single nanoparticles are highly sensitive to all details of their geometry. These geometric details play an important role in determining the utility of a nanoparticle as a sensor. It was demonstrated that nanoprisms have a 1 nm per $CH_2$ unit greater sensitivity to the binding of molecular adsorbates than truncated tetrahedral arrays despite being five times thinner, suggesting they will be excellent candidates for sensing large biomolecules. It was further shown, for the case of the nanocubes, that the energy of LSPR modes are not simply sensitive to their environments, but that the environment can actually affect the number of modes observed in a nanoparticle's LSPR spectrum. A figure of merit (FOM) has been defined for single-nanoparticle sensors, and the nanocubes' high-energy peaks were shown to have the highest-value FOM measured to date.**

***Index Terms*—Localized surface plasmon resonance (LSPR), resonant adsorbate, sensing, single-nanoparticle spectroscopy.**

## I. Introduction

PLASMONICS, an emerging branch of nanophotonics, is the study of light interacting with nanostructured materials that can support a surface plasmon resonance excitation. This excitation is a coherent oscillation of the surface conduction electrons excited by electromagnetic (EM) radiation [1]–[3]. The rapidly growing interest in plasmonics lies in its potential applications for highly miniaturized and sensitive photonic devices by controlling, manipulating, and amplifying light on the nanoscale [4], [5]. To date, a variety of plasmonic devices have been demonstrated, such as waveguides [5]–[8], photonic circuits [9], [10], filters [8], and nanoscopic light sources [11]. Furthermore, our rapidly improving understanding of the interactions between adsorbed molecules and plasmonic nanostructures (i.e., molecular plasmonics) is having a significant impact on a broad spectrum of other applications, including nanoscale optical spectroscopy [12], [13], surface-enhanced Raman spectroscopy (SERS) [3], [14], [15], and surface plasmon resonance sensing [16]–[18].

There are two types of surface plasmon excitations—surface plasmon polaritons (SPPs) and localized surface plasmon resonances (LSPRs). SPPs are propagating excitations that move along the metal–dielectric interface for distances of the order of tens to hundreds of micrometers. SPPs are associated with smooth, thin metal films. The interaction between the metal-surface-confined EM wave and an adsorbate layer leads to angle shifts in the plasmon resonance condition that are measured in surface plasmon resonance (SPR) measurements. LSPR excitation, by contrast, occurs in metal nanoparticles that are much smaller than the incident wavelength. Here, the induced polarization oscillates locally around the nanoparticle at a certain frequency. The LSPR wavelength ($\lambda_{\max}$) and peak width of the nanoparticles are extremely sensitive to nanoparticle composition [19], [20], size [21], shape [22]–[24], dielectric environment [25]–[28], and proximity to other nanoparticles [29]–[32].

Both SPR and LSPR are sensitive to the local refractive index changes that occur when a target analyte binds to the metal film or nanoparticles; therefore, a variety of chemical/biological sensors have been developed based on SPR and LSPR. These sensors are highly sensitive, label-free, and can provide real-time kinetic information for binding processes [33]. In addition, LSPR sensing elements are intrinsically at the single-nanoparticle level, making the LSPR sensors possible for *in situ* detection in biological systems. Furthermore, advances in synthetic and lithographic fabrication techniques allow for tuning the LSPR wavelength throughout the visible, near-infrared, and into the infrared region of the EM spectrum, by varying the shape, size, and material of the nanoparticles [20], [23], [25], [34]–[38]. This gives flexibility in designing and optimizing LSPR sensors.

This review will focus on recent progress in studying the coupling of resonant molecular layers and LSPR. We also

Manuscript received March 19, 2008; revised April 14, 2008. Current version published December 24, 2008. This work was supported in part by the Air Force Office of Scientific Research under MURI Program Grant F49620-02-1-0381, in part by the DTRA JSTO Program under Grant FA9550-06-1-0558, and in part by the National Science Foundation under Grant EEC-0647560, Grant CHE-0414554, Grant DMR-0520513, and Grant BES-0507036.

J. Zhao, G. C. Schatz, and R. P. Van Duyne are with the Department of Chemistry, Northwestern University, Evanston, IL 60208-3113 USA (e-mail: j-zhao4@northwestern.edu; schatz@chem.northwestern.edu; vanduyne@northwestern.edu).

L. J. Sherry is with the Center for Naval Analysis, Alexandria, VA 22311 USA (e-mail: sherryl@cna.org).

Color versions of one or more of the figures in this paper are available online at http://ieeexplore.ieee.org.

Digital Object Identifier 10.1109/JSTQE.2008.924840

explore single-nanoparticle spectroscopy, where the LSPR peak position and width are correlated with the nanoparticle structures. This research has been carried out from both experimental and theoretical perspectives. In the first part, the effect of a monolayer of resonant adsorbates on the LSPR of Ag nanoparticles was explored by mapping the LSPR wavelength shift upon the adsorption of the analytes through the visible wavelength region [39], [40]. This study has revealed the correlation between the molecular resonances and the nanoparticles' surface plasmon resonances for several different resonant adsorbates. When resonant molecules are adsorbed on the nanoparticles, strong coupling between the molecular resonance and nanoparticle LSPR has been observed experimentally and simulated by electrodynamics theory. The induced LSPR shift due to this coupling is found to be strongly dependent on the spectral overlap between molecular resonances and the LSPR. Moreover, the LSPR shift was found to be highly sensitive to the electronic structures of the adsorbed species [39]. Therefore, one can study the electronic structures of the adsorbates when interacting with metallic nanoparticle surface from the wavelength-dependent LSPR shift. This mechanism was applied to detect small substrate molecule (camphor) binding to the heme-containing cytochrome P450cam proteins (CYP101) that induce an electronic structure change in CYP101 [41].

In the second part, the study of single-nanoparticle LSPR spectroscopy is detailed by presenting results for single nanocubes and triangular nanoprisms [25], [34]. These studies have revealed a number of important factors affecting a nanoparticle's LSPR that were not revealed by studies of the ensemble. First, the effect of a dielectric substrate on the LSPR of single nanocubes was studied. The purpose of this study was to understand influences beyond that of the well-understood red-shift of the LSPR due to the generally higher refractive index of the substrate than that of the surrounding medium. It was observed that only nanoparticles with particular geometric features, specifically sharp tips, experience substantial perturbations to their LSPRs. Next, the effects of inhomogeneous and homogeneous broadening of the LSPR linewidth are studied for the case of triangular nanoprisms, where it was again found that the sharpness of the nanoparticles' tips is much more important than previously suspected. While all the factors discussed earlier are of interest from a fundamental perspective, we also discuss their impact on the utility of single nanoparticles as chemical and biological sensing platforms.

## II. Coupled Molecular and Plasmon Resonances

As discussed earlier, molecular plasmonics studies metal–adsorbate interactions for a variety of applications. To date, most LSPR studies have focused on the interaction between metal nanoparticles and nonresonant adsorbates that do not exhibit electronic transitions in the visible wavelength region. However, it is important to understand the interaction and electronic structure changes associated with resonant adsorbates and metallic nanostructures as these systems can play an active role in solar energy research [42]–[44], resonant SERS [45], [46], and plasmonic devices [47], [48]. In this section, we will review our progress in studying the mechanism and application of the coupling between molecular and plasmon resonances. We separate this section into three parts: 1) Section II-A deals with the observation and modeling of the wavelength-dependent LSPR shift induced by MgPz; 2) Section II-B deals with a further study regarding the interaction of Rhodamine 6G (R6G) with Ag nanoparticles, where the plasmon resonance lineshape is found to be highly sensitive to the electronic structure changes in R6G; and 3) Section II-C deals with a resonant LSPR sensor to detect substrate molecule binding to CYP101 that changes the electronic structure of CYP101.

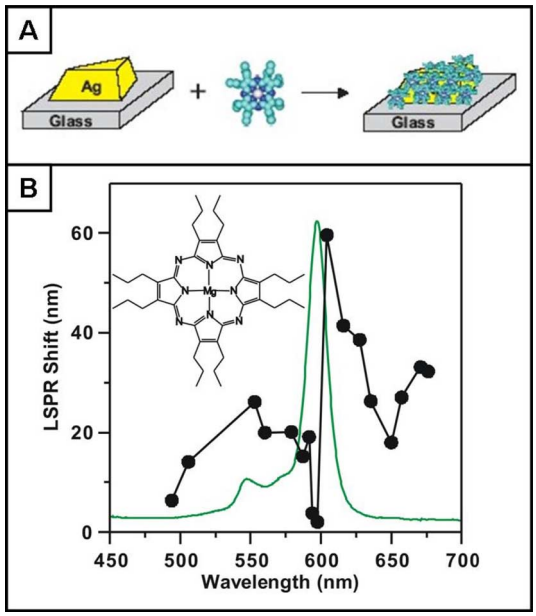


Fig. 1. (A) Schematic illustration of the experimental procedure. (B) Wavelength-dependent LSPR shifts induced by MgPz adsorption to Ag nanoparticles. Inset shows the molecular structure of MgPz. The solid green line is the solution absorption spectrum of MgPz. The black solid line with dots presents the induced LSPR shifts from a monolayer of MgPz versus the LSPR of bare Ag nanoparticles. Reproduced with permission from [40]. Copyright 2006 American Chemical Society.

### A. Wavelength-Dependent LSPR Shift Induced by MgPz

To study the effect of [2, 3, 7, 8, 12, 13, 17, 18-Octakis(propyl) porphyrazinato] magnesium (II) (MgPz) on the LSPR of Ag nanoparticles, nanoparticles with varying LSPR throughout $450 \sim 700$ nm were fabricated with nanosphere lithography (NSL) by controlling the in-plane widths and out-of-plane heights [21], [24]. Then, an ethanol solution of MgPz was introduced to the nanoparticle surface in a home-built flow-cell [26]. After 1 h incubation, the nanoparticles were thoroughly rinsed with excess ethanol and dried in $N_2$ [experimental scheme shown in Fig. 1(A)]. MgPz has $D_{4h}$ symmetry and contains a magnesium-centered porphyrazinato ring [structure shown in the inset in Fig. 1(B)]. This molecule has two features in its solution absorption spectrum that are both polarized within the plane of the molecule [spectrum shown in Fig. 1(B), green solid line]. There is a strong low-energy absorbance centered at 598 nm from $\pi$–$\pi*$ transition with a slightly higher energy shoulder at 548 nm [49]–[52].

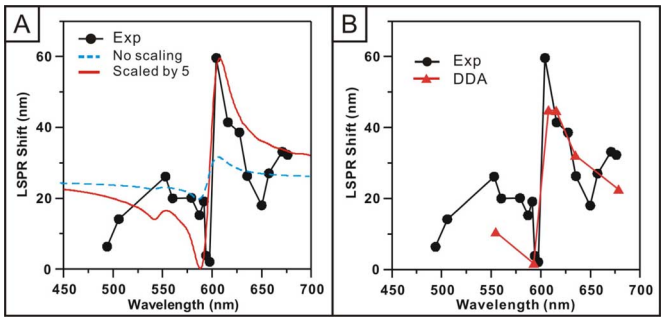


Fig. 2. Prediction of LSPR shift versus wavelength. (A) Predicted LSPR shift using (1) and refractive index calculated from Kramers–Kronig transformation. The solid black line with filled dots is a plot of the experimental LSPR shift (nm) versus spectral position of the Ag nanoparticles. Blue dashed line is calculated using the refractive index from Kramers–Kronig transformation. Red solid line is calculated using a scaled refractive index. (B) Predicted LSPR shift using DDA method. The solid black line with filled dots is a plot of the experimental LSPR shift (nm) versus spectral position of the Ag nanoparticles. The solid red line with filled triangles is the LSPR shift predicted by DDA method. Reproduced with permission from [40]. Copyright 2006 American Chemical Society.

The LSPR spectra of the nanoparticles before and after MgPz adsorption were monitored using UV-vis spectroscopy in $N_2$. The LSPR shift ($\Delta\lambda_{\max}$) was calculated from the difference in $\lambda_{\max}$ of bare and MgPz coated nanoparticles. The black solid line with dots in Fig. 2 reveals the effect of a monolayer of MgPz on the LSPR shift. At an off-molecular-resonance wavelength (<550 nm and >650 nm), an LSPR shift of ~20 nm was observed. However, when the nanoparticle LSPR is close to the molecular resonance, interesting behavior is observed. When an LSPR peak maximum directly overlaps with the molecular resonance, the LSPR shift is reduced to less than 2 nm. When the LSPR maximum is slightly red-shifted from the molecular resonance, the LSPR shift is amplified by 300% over the average LSPR shift (20 nm) to 60 nm. It is apparent that the LSPR shifts highly depend upon the extent of spectral overlap of the LSPR and molecular resonances.

Both empirical and electrodynamics modeling have been used to simulate the experimental results. An empirical model has been examined first. Previous studies have demonstrated that $\Delta\lambda_{\max}$ can be predicted using the following equation: [53]–[56]

$$\Delta\lambda_{\max} = m(n_{\text{ads}} - n_{\text{surr}})(1 - e^{-2d/l_d}) \tag{1}$$

where $m$ is the refractive index sensitivity of the nanoparticles [~200 nm/refractive index unit (RIU)] [26], [57], $n_{\text{ads}}$ is the refractive index of the adsorbed molecules, $n_{\text{surr}}$ is the refractive index of the surroundings ($N_2$ in this study with refractive index = 1.0), $d$ is the thickness of the adsorbed layer (experimentally determined to be 0.4 nm, data not shown), and $l_d$ is the characteristic electromagnetic field decay length of the nanoparticles (tunable but approximately 6 nm) [53]. For convenience, $n_{\text{ads}}$ is divided into two parts as $n_{\text{ads}} = n_{\text{non,ads}} + \Delta n_{\text{res,ads}}$, where $n_{\text{non,ads}}$ is the nonresonant portion of the refractive index and $\Delta n_{\text{res,ads}}$ is the resonant part. As discussed earlier, the average LSPR shift at off-molecular resonance wavelength is ~20 nm; therefore, $n_{\text{non,ads}}$ is calculated to be 2.0 using (1).

To calculate the resonant portion of the refractive index of the absorbing molecule, the Kramers–Kronig transformation is applied. The Kramers–Kronig treatment [58] calculates the real part of the refractive index from the imaginary part, which is directly related to the molecular absorption spectrum, using the following equation:

$$\Delta n_{\text{res,ads}}(\omega') = \frac{c}{\pi}\sum_{0}^{\infty}\frac{\Delta\alpha(\omega)}{\omega^2 - (\omega')^2}d\omega \tag{2}$$

where $\Delta\alpha$ is the change in the absorption coefficient ($2.303 \times A(\lambda)/T$, $A(\lambda)$ is the molecular absorbance at a given wavelength, and $T$ is the effective molecular thickness), $c$ is the speed of light, $\lambda$ is the wavelength of light, and $\omega$ is the angular frequency ($2\pi c/\lambda$).

From (2) and the solution absorption measurement of MgPz, the real part of the refractive index is calculated to be $-0.198 < \Delta n_{\text{res,ads}} < 0.276$. Consequently, $n_{\text{ads}}$ is between 1.802 and 2.276. Therefore, the LSPR peak shift (from (1)) is calculated to be $20.0\text{ nm} \leq \Delta\lambda_{\max} \leq 31.8\text{ nm}$ and plotted as the blue dashed line in Fig. 2(A). From the comparison to experimental data [Fig. 2(A)], the predicted line shape tracks the experimental results; however, the magnitude of the shift is severely underestimated. Scaling by 5 is performed by modifying $n_{\text{ads}}$ as $n_{\text{ads}} = n_{\text{non,ads}} + 5 \times \Delta n_{\text{res,ads}}$ in order to match the experimental LSPR shifts. Using (1), the scaled LSPR shift is calculated and shown in Fig. 2(A), red solid line. It is clear that with a scaling factor of 5, the predicted LSPR shifts agree well with both the line shape and the magnitude of the experimental LSPR shifts. Note that solution absorption measurements are used in the Kramers–Kronig transformation while the LSPR shift measurements are performed with the molecules adsorbed onto the nanoparticle surfaces. Therefore, the scaling can be understood based on a surface-induced change in the absorption coefficient. Physically, when the molecules adsorb to the nanoparticles, they should be aligned on the surface; whereas, in solution, they will be randomly oriented. Alignment of the adsorbates could produce transition moments that are not orientation-averaged, which should lead to an enhancement in effective absorption coefficient of roughly a factor of 3 (the inverse of the average of $\cos^2\theta$). Additional enhancement in the absorption coefficient can arise from electronic coupling between the molecule and metal [40].

The empirical modeling with the scaled refractive index of MgPz agrees well with the experimental results. In an attempt to understand these data more quantitatively, electrodynamics modeling was performed using the discrete dipole approximation (DDA) method. DDA is a finite-element-based approach to solving Maxwell's equations for light interacting with an arbitrary shape/composition nanoparticle in various dielectric environments [22], [59]. DDA calculations were performed for truncated tetrahedron Ag particles (dielectric constants from Lynch and Hunter [60]) in which the particle width and height were varied to tune the LSPR through the molecular resonance. To obtain the LSPR shift, the LSPR wavelength of bare silver was first calculated, and then the MgPz layer was added (refractive index from the scaled Kramers–Kronig analysis) to get the LSPR of the nanoparticle with adsorbates. Note that the thickness of the MgPz layer used in these studies is 2 nm, which

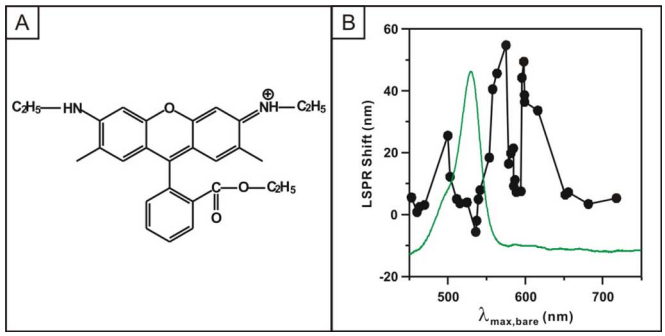


Fig. 3. (A) R6G molecular structure. (B) R6G absorption and wavelength-dependent LSPR shift induced by a monolayer of R6G versus the LSPR wavelength of bare Ag nanoparticles. The green solid line is the absorption spectrum of the R6G in ethanol solution (arbitrary scaling). Solid black line with filled dots is a plot of the LSPR shift (nm) versus LSPR position of Ag nanoparticles. Reproduced with permission from [39]. Copyright 2007 American Chemical Society.

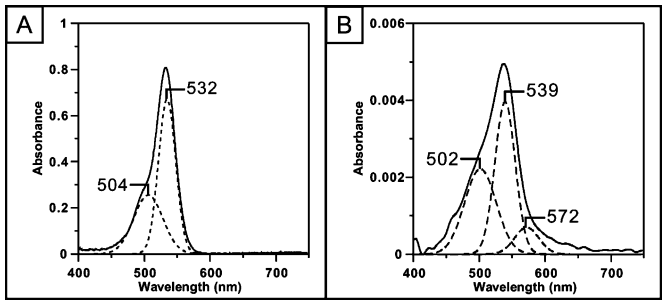


Fig. 4. (A) Absorption spectra of 6 $\mu$M R6G in ethanol solution. (B) Thin layer of R6G on a Ag surface. Dashed lines represent deconvolution of the spectra into Gaussian bands. Reproduced with permission from [39]. Copyright 2007 American Chemical Society.

is larger by a factor of 5 compared to the measured thickness (0.4 nm), thereby incorporating another scaling factor of 5 comparing to the Kramers–Kronig analysis. Thus, in order to get quantitative agreement with the experimental results, the DDA calculations need to overestimate the layer thickness of MgPz.

Results from the DDA calculations together with the experimental data are shown in Fig. 2(B). Comparing Fig. 2(A) and Fig. 2(B), the predicted LSPR shifts are similar to what was obtained using (1) with the same scaled refractive index. This confirms that (1) provides a useful empirical parameterization of the LSPR shift. In addition, it shows that the previously derived scaling factor is necessary for generating results that match the experimental results quantitatively.

This study shows that the LSPR shift induced by resonant adsorbates is strongly dependent on the spectral overlap between the electronic resonance of the adsorbates and the plasmon resonance of the nanoparticles. A reduced response is observed when the LSPR directly overlaps with the adsorbate's molecular resonance. Meanwhile, an amplified shift occurs when the nanoparticles' LSPR is located at a slightly longer wavelength than the molecular resonance.

### *B. Interaction of R6G Molecular Resonances With Ag Nanoparticles' Plasmons*

R6G is one of the first and most widely studied molecules in single-molecule SERS (SMSERS) [45], [46]. Understanding the interaction of R6G and Ag nanoparticles is crucial for elucidating the single-molecule SERS mechanism. By exploring the wavelength-dependent LSPR shift induced by R6G, one can obtain a microscopic understanding of R6G–Ag nanoparticle interaction.

Fig. 3 inset shows the structure of R6G and the green line is its solution absorption spectrum. In ethanol solution, R6G exhibits a peak at 530 nm from the $S_0$-$S_1$ electronic transition and a shoulder at 495 nm from vibronic $S_0$-$S_1$ transition [61], [62]. Following the same experimental scheme as in Fig. 1(A), the influence of a monolayer of R6G on the LSPR of Ag nanoparticles was studied.

When scanning wavelength shift versus plasmon wavelength for $\lambda_{\max,\mathrm{bare}}$ from 450 to 750 nm, the LSPR shift shows interesting and more complicated behavior compared to the previously discussed case of MgPz. As shown in Fig. 3, when $\lambda_{\max,\mathrm{bare}}$ is much bluer (i.e., 450 $\sim$ 470 nm) than the molecular resonance, a small LSPR shift (less than 5 nm) is observed. As $\lambda_{\max,\mathrm{bare}}$ is gradually tuned to the red, the LSPR shift increases and a local LSPR shift maximum of 25 nm occurs at $\lambda_{\max,\mathrm{bare}} \sim 500$ nm. When $\lambda_{\max,\mathrm{bare}}$ approaches the R6G resonance, the LSPR shift decreases and drops to a slight blue shift ($\sim$5 nm) at 530 nm. When $\lambda_{\max,\mathrm{bare}}$ is red-shifted from the molecular resonance, the LSPR shift recovers and reaches a maximum of 55 nm at $\lambda_{\max,\mathrm{bare}} \sim 575$ nm. Similar to MgPz, this maximum response is amplified by $\sim$300% over the average LSPR shift ($\sim$20 nm). As $\lambda_{\max,\mathrm{bare}}$ is further red-shifted from 575 to 590 nm, the LSPR shift sharply drops to less than 10 nm followed by another LSPR shift maximum ($\sim$50 nm) at $\lambda_{\max,\mathrm{bare}} \sim 595$ nm. Finally, when $\lambda_{\max,\mathrm{bare}}$ is red-shifted past 595 nm, the LSPR shift slowly decreases to less than 10 nm at $\lambda_{\max,\mathrm{bare}} > 700$ nm. It is particularly noteworthy that three LSPR shift local maxima at 500, 575, and 595 nm were observed while there are only two features observed in the R6G absorption spectrum.

As discussed, R6G has two absorption features in ethanol solution—an $S_0$-$S_1$ electronic transition and a vibronic shoulder. Fig. 4(A) shows the deconvolution of the R6G solution phase absorption spectrum with two Gaussian curves at 532 and 504 nm. Since all the R6G induced LSPR shift measurements were conducted on an Ag surface with nanoscale patterns, it is important to examine the absorption behavior of R6G on an Ag surface.

A 200-nm-thick Ag film on glass was prepared by thermal deposition. The film was then incubated in R6G solution for 2–4 h and rinsed thoroughly. The absorbance of R6G was measured in reflectance geometry using an integrating sphere. Fig. 4(B) shows the absorbance of R6G on an Ag surface. R6G is known to form dimers in solution at high concentrations and when intercalated in heterogeneous materials like clays, silica, and colloidal gold nanoparticles [63]–[68]. R6G can form both J-type (head-to-tail dipole moments) and H-type dimers (parallel dipole moments). The formation of dimers will affect the absorption characteristics of R6G by inducing spectral shifts and band splitting. From exciton theory [69], [70], the H-dimer absorption is blue-shifted from the R6G monomer absorption whereas the J-dimer absorption is red-shifted. Fig. 4(B) shows the deconvolution of the absorption spectrum using three

Gaussian curves at 502, 539, and 572 nm with correlation coefficients greater than 0.99. The peak at 539 nm has the highest intensity, followed by the curve at 502 nm, and the lowest intensity at 572 nm. From a series of experiments conducted with different R6G dosing concentrations (data not shown), we conclude that the three peaks at 502, 539, and 572 nm are associated with R6G H-dimer, monomer, and J-dimer, respectively.

We hypothesize that the R6G H-dimer, monomer, and J-dimer correspond to the three LSPR shift maxima. To examine this hypothesis, we use quasistatic (Gans) theory as a simplified model [71]. The extinction cross section $C_{\text{ext}}$ of a metallic particle in a homogenous medium is expressed as: [71], [72]

$$C_{\text{ext}} \propto \text{Im}\left\{\frac{\varepsilon_{\text{Ag}} - \varepsilon_m}{\varepsilon_{\text{Ag}} + \chi\varepsilon_m}\right\} \tag{3}$$

where $\varepsilon_{\text{Ag}}$ is the dielectric constant of Ag, $\varepsilon_m$ is the dielectric constant of the surrounding medium, and $\chi$ is a shape factor for the particle that is 2 for a sphere, and increases with increasing aspect ratio. In this model, $\chi$ is used as a parameter to tune the plasmon resonance wavelength, so the quantitative connection between $\chi$ and the structure of the particle is not needed. For the bare Ag particle, $\varepsilon_m$ is set as 1 for $N_2$. When $\chi$ varies from 2.0 to 24.0, the extinction maximum wavelength of the bare Ag particle ($\lambda_{\text{max,bare}}$) varies from 400 to 750 nm. As mentioned earlier, we assume that one of the three R6G species dominates the LSPR shift at each wavelength; therefore, $\varepsilon_m$ for the adsorbates ($\varepsilon_{m,\text{ads}}$) is expressed as

$$\varepsilon_{m,\text{ads}} = \begin{cases} \varepsilon_{H,} & 400 < \lambda_{\text{max,bare}} < 530 \\ \varepsilon_{\text{mon},} & 530 < \lambda_{\text{max,bare}} < 570 \\ \varepsilon_{J,} & 570 < \lambda_{\text{max,bare}} < 750 \end{cases} \tag{4}$$

where $\varepsilon_H, \varepsilon_{\text{mon}}$, and $\varepsilon_J$ are the dielectric constants of the R6G H-dimer, monomer, and J-dimer, respectively. Values for these dielectric constants were obtained by the Kramers–Kronig transformation (2) with arbitrary scaling factors to match the experimental results.

Fig. 5 shows the predicted LSPR shift versus $\lambda_{\text{max,bare}}$. The blue dashed-dotted line, red dotted line, and green dashed line represent the LSPR shift from the dielectric constants of the R6G H-dimer, monomer, and J-dimer, respectively. The prediction agrees well with the experimental data thus confirming that the three LSPR shift features are associated with R6G in the three different forms.

This study demonstrates the extreme sensitivity of the LSPR wavelength to small environmental changes. Changes in the adsorbates' electronic structure due to aggregation have been detected using LSPR spectroscopy. These findings show that the LSPR sensing technique is particularly suitable for studying molecular-level information, such as electronic and structural change of the adsorbates.

### *C. Detection of the Low Molecular Weight Substrate Binding to Cytochrome P450 Protein Based on the LSPR Response Near Molecular Resonance*

The resonant LSPR response discussed earlier opens the possibility of detecting electronic structure changes in resonant biological systems. With guidance from the resonant LSPR studies, it is possible to design a protein receptor adsorbed on nanoparticle surface, and optimize the sensor to detect molecules that can induce electronic structure changes in the protein. Specifically, we choose cytochrome P450cam protein (CYP101) and a low molecular weight substrate molecule, camphor ($C_{10}H_{16}O$, molecular weight $= 152.24\ \text{g} \cdot \text{mol}^{-1}$) as a model system.

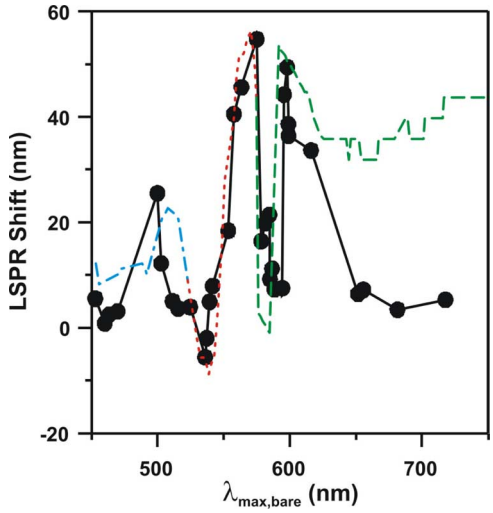


Fig. 5. Predicted LSPR shift using (3). The solid black line with filled dots is a plot of the experimental LSPR shift (nm) versus spectral position of the Ag nanoparticles. The blue dashed-dotted line, red dotted line, and green dashed line represent the predicted LSPR shift using the dielectric constants of the R6G H-dimer, monomer and J-dimer, respectively. Reproduced with permission from [39]. Copyright 2007 American Chemical Society.

CYP101 is a heme-containing protein belonging to the P450 superfamily. When camphor binds to CYP101, it displaces the water coordinated with the heme-iron and shifts the iron center from the low-spin to the high-spin state. This spin state change results in a 26-nm blue-shift in the Soret absorption band from 417 nm (extinction coefficient $\varepsilon = 115\ \text{mM}^{-1} \cdot \text{cm}^{-1}$) to 391 nm ($\varepsilon = 102\ \text{mM}^{-1} \cdot \text{cm}^{-1}$) [73], [74].

Fig. 6(A) schematically illustrates the LSPR sensing scheme. Ag nanoparticles were fabricated by NSL and functionalized with a self-assembled monolayer (SAM) of 11-mercaptoundecanoic acid (11-MUA) by incubating the nanoparticles in 1-mM 11-MUA solution overnight. CYP101 proteins were immobilized covalently on the SAM-functionalized nanoparticle surface with the aid of 1-Ethyl-3-[3-dimethyaminopropyl]carbodiimidehydrochloride [54]. Finally, the sample was exposed to a 200-$\mu$M camphor solution. The sample was rinsed carefully with excess solvent after each binding step. The LSPR of the sample during each experimental step was monitored using UV-vis extinction spectroscopy in an $N_2$ environment.

The LSPR response to protein and substrate binding is expected to be wavelength-dependent. Therefore, Ag nanoparticles with various LSPRs were tested. For convenience, $\lambda_{\text{max,SAM}}$, $\lambda_{\text{max,CYP101}}$, and $\lambda_{\text{max,CYP101-Cam}}$ denote the LSPR wavelength of SAM-functionalized Ag nanoparticles after CYP101 immobilization, and after camphor binding,

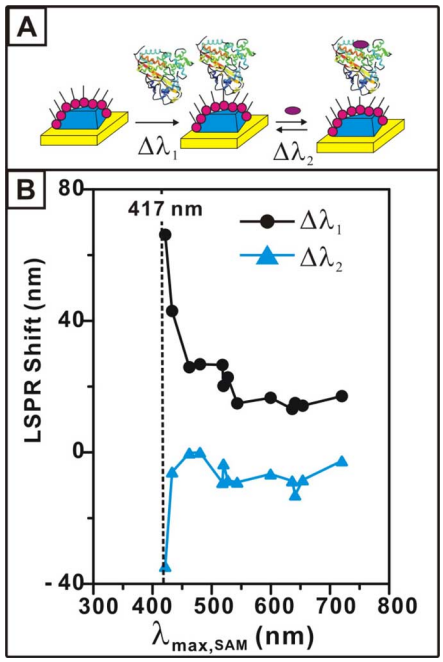


Fig. 6. Substrate binding detection scheme and LSPR shift. (A) Schematic representation of CYP101 protein immobilized Ag nanobiosensor, followed by binding of camphor. (B) Plots of LSPR shifts versus $\lambda_{\mathrm{max,SAM}}$, where $\Delta\lambda_1 = \lambda_{\mathrm{max,CYP101}} - \lambda_{\mathrm{max,SAM}}$ (shift on binding CYP101) and $\Delta\lambda_2 = \lambda_{\mathrm{max,CYP101\text{-}Cam}} - \lambda_{\mathrm{max,CYP101}}$ (shift on binding camphor). The vertical black dotted line denotes the molecular resonance of $Fe^{3+}$ CYP101 at 417 nm. Reproduced with permission from [41]. Copyright 2006 American Chemical Society.

respectively. The LSPR response upon CYP101 binding ($\Delta\lambda_1$) was calculated from $\Delta\lambda_1 = \lambda_{\mathrm{max,CYP101}} - \lambda_{\mathrm{max,SAM}}$ and the response from camphor binding ($\Delta\lambda_2$) was calculated using $\Delta\lambda_2 = \lambda_{\mathrm{max,CYP101\text{-}Cam}} - \lambda_{\mathrm{max,CYP101}}$. Fig. 6(B) shows the LSPR response of $\Delta\lambda_1$ (black line with dots) and $\Delta\lambda_2$ (blue line with triangles) versus $\lambda_{\mathrm{max,SAM}}$.

From Fig. 6(B), $\Delta\lambda_1$ is positive for all different $\lambda_{\mathrm{max,SAM}}$ corresponding to a red-shift; while $\Delta\lambda_2$ is negative ($-$) meaning a blue-shift. Note that similar to the previous studies of nonresonant proteins, the LSPR red-shifts from $\lambda_{\mathrm{max,SAM}}$ upon binding of either CYP101, or camphor-bound CYP101. However, when camphor binds to CYP101, it induces a blue-shift in the LSPR; in other words, $\lambda_{\mathrm{max,CYP101\text{-}Cam}}$ is blue-shifted relative to $\lambda_{\mathrm{max,CYP101}}$. It is unusual that addition of an analyte leads to a blue-shift of the LSPR. If camphor were a noninteracting adsorbate added to CYP101, the local refractive index around the nanoparticles would increase, resulting in a red-shift in the LSPR. However, blue-shifts were observed for a variety of nanoparticles with different $\lambda_{\mathrm{max,SAM}}$ [Fig. 6(B)]. This indicates that substrate binding to CYP101 involves a change in the electronic state of the protein.

When the $\lambda_{\mathrm{max,SAM}}$ is at an off-resonance wavelength for CYP101 (>460 nm), an average shift of ~19 nm is observed for $\Delta\lambda_1$, and ~$-$6 nm for $\Delta\lambda_2$. However, when $\lambda_{\mathrm{max,SAM}}$ is tuned to be closer to the CYP101 resonance, $\Delta\lambda_1$ increases. When $\lambda_{\mathrm{max,SAM}}$ is at a slightly longer wavelength than the CYP101 resonance (~420 nm), amplified shifts are observed for $\Delta\lambda_1$ (amplified magnitude ~340%) and $\Delta\lambda_2$ (~550%). Amplified LSPR response is achieved for resonant biological systems as well as the dye molecules.

## III. Single-Nanoparticle Spectroscopy

As discussed earlier in Section I, this section will address our efforts to understand the plasmonic properties of single nanoparticles by detailing our research on nanocubes and triangular nanoprisms. Research in the field of single-nanoparticle LSPR spectroscopy has consisted almost entirely of discussions of colloidal nanoparticles (i.e., spherically shaped nanoparticles), with a few notable exceptions [75], [76]. Investigations into how the detailed structure of single nanoparticles sharing a similar overall geometry (triangular prisms with slightly different thicknesses, edge lengths, and tip sharpness for example) affects their individual LSPR and the LSPR of an ensemble of such subtly diverse nanoparticles have been lacking. Also lacking is an understanding of how these geometric subtleties can affect the interaction of a nanoparticle's LSPR with its environment. It will be shown in the subsequent sections that these considerations are not trivial when using these systems as platforms for chemical sensing. We separate this section into three parts: 1) substrate effects on the LSPR of single silver nanocubes; 2) LSPR spectroscopy of single silver triangular nanoprisms; and 3) sensing with single nanoparticles.

### *A. Substrate Effects on the LSPR of Single Silver Nanocubes*

Intrinsic to many types of optical studies and applications in nanoscience is the need to immobilize nanoparticles on a substrate. In this study, the influence of a dielectric substrate on the LSPR spectra of single silver nanocubes is investigated to show how the nanocube LSPR spectra are uniquely altered due to the presence of such a substrate. In contrast to earlier research [77], [78], this study involves measurements on single particles rather than an ensemble, thereby removing the effect of averaging, and enabling us to observe previously unsuspected details of the effects of substrate interactions. Here, transmission dark-field spectroscopy is used to interrogate the nanoparticles.

Fig. 7 shows that there are *two* plasmon resonance peaks when a silver cube interacts with a glass substrate, one of which is red-shifted relative to the bulk spectrum (where only a single peak is observed), and the other being blue-shifted and considerably narrower. The blue-shifted resonance was not anticipated based on earlier study with the particles in solution, but finite-difference time-domain electrodynamics calculations (FDTD) [79] confirm that this is the expected result for this nanoparticle geometry.

Fig. 8 explains why this is the expected LSPR response for a nanocube in contact with a glass substrate. A series of calculations for a nanocube at various heights above a glass substrate surface were performed, and it was observed that the LSPR response gradually shifts from a single resonance, which is expected for a geometry of such high symmetry, to two distinct resonances [Fig. 8(A)]. This previously unobserved phenomenon can be understood in terms of the pattern of the locally enhanced fields induced by the LSPR [Fig. 8(B) and (C)]. For the case of a

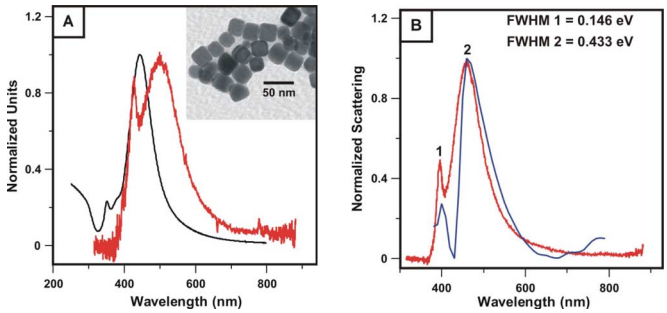


Fig. 7. Comparison of the LSPR spectra of the following. (A) Nanocube ensemble extinction (black) and single nanocube dark-field scattering (red) in $H_2O$ environment. (B) Single nanocube dark-field scattering (red) and FDTD theory (blue) in a nitrogen environment. Reproduced with permission from [25]. Copyright 2005 American Chemical Society.

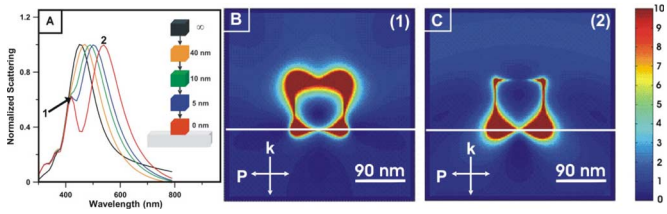


Fig. 8. FDTD theory showing the following. (A) Emergence of a second peak as a single nanocube (90 nm diameter) approaches a dielectric substrate. (B) and (C) Field intensities for peaks 1 and 2 of the nanocube in contact with the substrate (the white line in the field pattern images represents the substrate). Reproduced with permission from [25]. Copyright 2005 American Chemical Society.

nanocube, the regions of highest field intensity reside in the "polar" regions (top and bottom of the nanocube relative to the electromagnetic field propagation direction) of the nanocube. This is in contrast to earlier studies of spherical nanoparticles [22], where it is the "equatorial" region along the polarization direction where the highest fields occur. This is a consequence of the tips present in the cubic structure. These tips concentrate the induced polarization, thereby increasing the electric field intensity around them. As a result, a nanocube effectively feels two different dielectric environments; the dynamic solvent environment above the nanocube, which influences the fields excited at the top of the nanocube (resulting in the higher energy peak), and the static substrate environment below the nanocube, which influences the fields excited at the bottom of the nanocube (resulting in the lower energy peak). Interestingly, FDTD analysis indicates that in order to observe a similar effect for a spherical nanoparticle, the structure must be embedded with half its volume in the substrate such that the equatorial region of the sphere is at the interface. Sharp tips, however, are not the only requirement to observe this effect. FDTD calculations showed that if a nanocube was thinner than the skin depth (~30 nm for silver), only one LSPR peak was observed. It is for this reason that the triangular nanoprims to be discussed in the following section do not show this effect (nanoprism thickness is ~10–15 nm) even though they have sharp features.

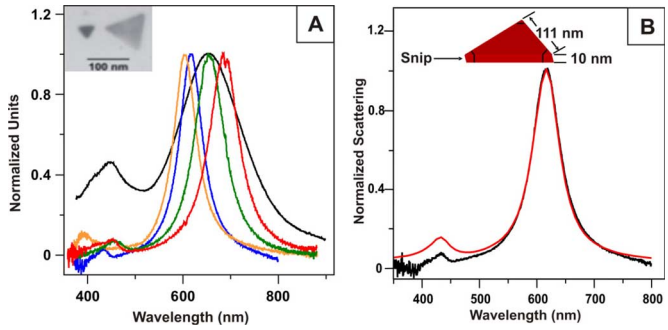


Fig. 9. LSPR spectra of silver triangular nanoprisms: (A) Ensemble extinction spectrum (black curve) versus single nanoparticle dark-field scattering spectra (colored curves) of triangular nanoprisms (representative nanoprisms shown in TEM inset). (B) Theoretical modeling (red curve) of a single triangular nanoprism using the DDA method. The theoretical spectrum was calculated for a nanoprism with edge length = 111 nm, snip = 15 nm, and height = 10 nm. Reproduced with permission from [34]. Copyright 2006 American Chemical Society.

### B. LSPR Spectroscopy of Single Silver Triangular Nanoprisms

The ability to synthesize triangular prisms by wet chemical techniques, pioneered by Mirkin and coworkers [38], elicited much excitement. This was in large part due to their potential use as chemical sensors and SERS substrates as well as their geometric similarity to the already successful nanosphere-lithography-derived truncated tetrahedral nanoparticles [16], [54], [80], [81]. In this study, the properties of single silver triangular nanoprisms are studied and compared with those of the ensemble.

This type of study is necessary since all nanoparticle suspensions contain geometric heterogeneity, which is the cause of inhomogeneous linewidth broadening in the ensemble LSPR spectra. Hence, in order to understand how the LSPR is affected by structural changes in detail, one must study single nanoparticles.

Fig. 9 illustrates this fact quite nicely. Panel A compares the ensemble LSPR spectrum with four single-nanoprism LSPR spectra. All the spectra display two LSPR resonances. These are the well-known in-plane dipole (lower energy peak) and the in-plane quadrupole (higher energy peak) [38]. There are two points to note when comparing the ensemble spectrum with the single-particle spectra: 1) the single-nanoprism spectra are ~4× narrower than the ensemble spectrum and 2) the single-particle resonances span the energies of the ensemble resonances. The second point is a result of differences in the geometries of the nanoprisms responsible for these spectra. While the LSPR peak positions span a range of up to 60 nm, this does not imply huge geometric differences in the structure of the nanoprisms. In fact, calculations using the DDA show that snipping off an 1-nm equilateral triangle from the tips of a perfectly formed nanoprism will shift the in-plane dipole LSPR mode ~5 nm lower in energy. Edge length and thickness changes will also shift the energies of the LSPR modes. Hence, modeling these systems can be a challenge.

Fig. 9(B) demonstrates the DDA method's ability to model the LSPR spectra of a single nanoprism. In this case, detailed structural information about the specific nanoprism yielding this

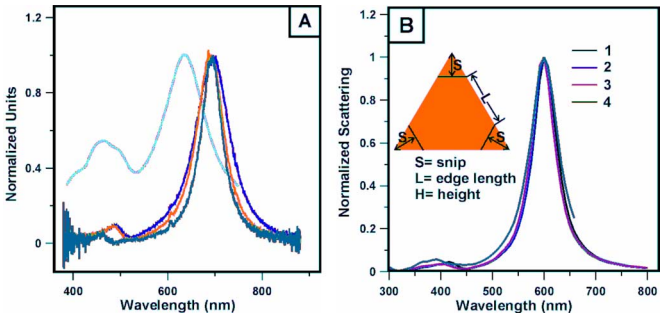


Fig. 10. (A) Ensemble extinction spectrum (gray curve) versus single nanoparticle LSPR scattering spectra of silver triangular nanoprisms. (B) Compares constant height versus changing size and snip. Dimensions (nm) are particle 1: L = 100, H = 10, and S = 11.5; particle 2: L = 90, H = 10, S = 7.5; particle 3: L = 80, H = 10, S = 3.5; particle 4: L = 70, H = 10, S = 0. Reproduced with permission from [34]. Copyright 2006 American Chemical Society.

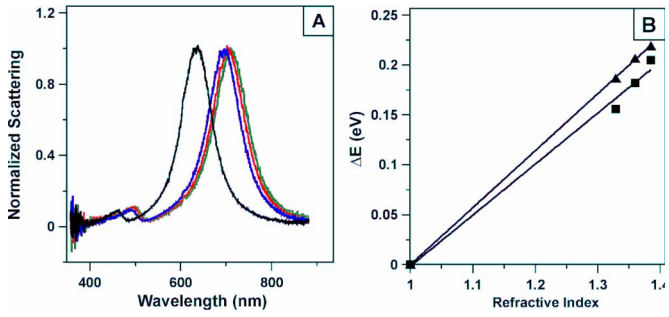


Fig. 11. (A) Single nanoprism dark-field scattering spectra in four different dielectric environments (refractive indexes = 1.000297, 1.329, 1.359, and 1.383) demonstrating the nanoprism's sensitivity to its environment. (B) Linear regression fit to the experimental data. Triangles represent dipole data ($m = 0.571\,\mathrm{eV\,RIU^{-1}}$, $R^2 = 0.999$) and squares represent = quadrupole data ($m = 0.512\,\mathrm{eV\,RIU^{-1}}$, $R^2 = 0.992$). Reproduced with permission from [34]. Copyright 2006 American Chemical Society.

LSPR spectrum was not available. Therefore, the structural parameters for the DDA model were varied until the peak positions were matched.

We are also very interested in understanding the factors affecting the LSPR linewidth, and it is interesting that the linewidths of the peaks in the spectrum generated by DDA match so well with experiment. The DDA method does not account for intrinsic [82], [83] linewidth broadening mechanisms (surface scattering). The excellent agreement between theory and experiment suggests this is not an important mechanism for the particles studied here. Another possible mechanism affecting plasmon linewidth is radiative damping (an extrinsic effect) [82], [83] in which case the plasmon linewidth increases with increasing particle size. For spherical particles, this effect scales with the square of the volume of the particle, and it becomes important for particles with diameters larger than 100 nm. Our DDA calculations also show that the linewidth does not increase with increasing edge length (considering edges in the 80–200 nm range) or with particle height (for 8–15 nm heights).

In contrast to these results, Fig. 10(A) shows that varying plasmon linewidths can be found experimentally at a single energy. This can be understood based on the DDA calculations in Fig. 10(B). In all the calculations, we kept the plasmon peak position constant since it is common for linewidths to vary across the spectrum due to more efficient coupling to dephasing pathways at different energies. DDA shows that nanoprisms with snipped tips have narrower linewidths. This effect can be understood in terms of the well-known lightening-rod effect.

### C. Sensing With Single Nanoparticles

The relationship between nanoparticle geometry and plasmonic properties, as discussed in the last section, is important beyond a fundamental understanding of these systems. These relationships can have a large influence on how nanoparticles are employed in technological applications. The application we will focus on in this section is utilizing single nanoparticles as small volume, ultrasensitive chemical sensors.

These studies exploit the environmental sensitivity of a nanoparticle's LSPR spectrum by exposing a nanoparticle to

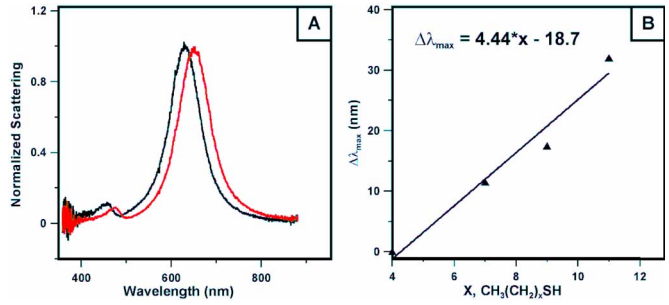


Fig. 12. LSPR dark-field scattering spectra of single silver nanoprisms before (black) and after (red) surface modification. (A) With 1-hexadecanethiol (5-nm dipole shift; BSPP capped). (B) With 1-decanethiol (19.84 nm shift; citrate capped). (C) Plot depicting the linear relationship between the LSPR response and the SAM alkyl chain length. Reproduced with permission from [34]. Copyright 2006 American Chemical Society.

solvents of varying refractive index or by modifying a nanoparticle's surface with a self-assembled monolayer (SAM) of small-molecule adsorbates [13], [34]. Figs. 11 and 12 show results for each of these types of sensing experiments for the case of triangular nanoprisms. Fig. 11 shows the typical LSPR response of a nanoprism to changes in its bulk dielectric environment. We note that this is the first system for which the systematic response of a quadrupole LSPR resonance to changes in its environment has been measured. The response is always linear with a slope smaller than that of the dipole resonance response.

Fig. 12 shows the response of a nanoprism to changes in its local environment. Fig. 12(A) shows the shift for decanethiol, and Fig. 12(B) demonstrates the sensitivity of these nanoparticles to adsorbing molecules of different chain lengths. This is possible for these systems due to the decay length of the locally enhanced fields that define the sensing volume for any nanoparticle sensor [57], [84], [85]. As more and more of the field's volume is filled by molecules that are of a different refractive index than the bulk environment, one observes a larger shift. The nanoprisms experience a 4.44 nm shift per $CH_2$ group. This is a 25% increase in molecular chain length sensitivity over colloidal single nanoparticles [13] and arrays of truncated tetrahedra [26]. This improvement in sensitivity is even more striking when one

considers the thickness of these particles relative to these other two types. The nanoprisms are at least five times thinner than the colloids or the truncated tetrahedra. This is important because the height of the local fields above the nanoparticle (i.e., its sensing volume) varies inversely with particle height. This means that the nanoprisms have achieved a 25% increase in sensitivity while utilizing a smaller fraction of their sensing volume.

Most of the studies in this area have focused on the value of the shift experienced by the plasmon resonance, and it has been shown that nanoparticles with sharp tips experience larger shifts than particles without sharp tips [57]. This can be explained by the localization of the enhanced near-fields near the tips as discussed in Section III-A. Hence, the sharper the tips, the larger the LSPR shift due to molecular binding. This is not, however, the only design rule for nanoparticle sensors to consider. As we saw in the last section, sharper tips lead to broader LSPR resonances. Hence, even though the magnitude of the LSPR shift due to molecular binding will increase with tip sharpness, there will be an accompanying broadening of the LSPR resonance. This broadening reduces the sensor's ability to resolve small shifts in the LSPR peak position. Therefore, one must be cognizant of these properties in order to optimize a sensor for a specific target. To account for both these factors in a general form, we have defined a figure of merit (FOM) so that we may more accurately compare the sensing performance of various nanoparticle geometries directly

$$\mathrm{FOM} = \frac{m(\mathrm{eV\,RIU}^{-1})}{\mathrm{FWHM\,(eV)}} \tag{5}$$

where $m$ is the nanoparticle's refractive index sensitivity, and FWHM is the nanoparticle's LSPR linewidth as measured at its full-width at half-maximum. For the specific examples of the nanoparticles discussed here, the nanocubes yield FOMs of 4–5 while the nanoprisms have FOMs of 2–3.

From (1), the sensitivity of a nanoparticle to an adsorbed molecular layer is determined by the FOM of the nanoparticle and the ratio of the thickness of the adsorbed layer ($d$) and the characteristic electromagnetic field decay length of the nanoparticles ($l_d$, sensing volume). This can be used to define a weighted FOM (WFOM) expressed as

$$\mathrm{WFOM} = \mathrm{FOM}(1 - e^{-2d/l_d}) \approx \mathrm{FOM}\frac{2d}{l_d} \tag{6}$$

where the second expression applies to adlayers that are smaller than the decay length. Equation (6) indicates that to achieve a large WFOM for a given adsorbate, it is the ratio of FOM to $l_d$ that needs to be optimized. For small molecules that only occupy a small fraction of the sensing volume, $d/l_d$ plays an important role in determining the WFOM and small particles, such as the cubes we have studied, are to be preferred; while for large molecules such as biomolecules, where most or all of the sensing volume is occupied, the WFOM is determined mostly by the FOM, and the nanoprisms are to be preferred.

SPR sensors based on metallic thin films have a characteristic electromagnetic field decay length of $\sim$200 nm, which in combination with their superior index of refraction sensitivity ($\sim 10^6$) makes them great for bulk refractive index or larger biological systems as a sensing platform. Nanoparticle-based sensors have lower index sensitivity, but a smaller decay length, so the advantage of SPR is less significant for measurements on small molecules. Another issue is that the surface area needed for SPR measurements is much larger than for LSPR, so the sensitivity per molecule of LSPR can often be better than SPR. In addition to nanocubes and nanoprims, many other nanostructures (nanoshells [86] and nanorods [87]) have been synthesized and can be used as potential LSPR sensors. The analysis based on (6) provides a general approach to comparison of the sensing abilities of these structures.

## IV. Conclusion

In this review, we discussed our latest progress in molecular plasmonics and single-nanoparticle spectroscopy. With regard to molecular plasmonics, we explored the effect of molecular electronic resonances on the LSPR wavelength for Ag nanoparticles from both experimental and theoretical points of view. By mapping the LSPR extinction maxima of Ag nanoparticles throughout the visible wavelength region, new phenomena were revealed. The LSPR shift induced by resonant adsorbates has a strong dependence on wavelength. When the LSPR of the nanoparticles is distant from the molecular resonance wavelength, the LSPR shift remains relatively constant. A reduced LSPR shift occurs when the nanoparticles' LSPR directly overlaps with the molecular resonance. An amplified response occurs when the LSPR is at a slightly longer wavelength than the molecular resonance. While the lineshape of the LSPR shift versus LSPR wavelength of the bare nanoparticles qualitatively tracks the Kramers–Kronig transformation of the molecular resonance spectrum (real portion of the refractive index) for the MgPz molecule, the magnitude of the response is underestimated. This was verified in both empirical model calculations based on (1) and in the DDA calculations. It suggests that the molecular absorption intensity is enhanced by surface adsorption.

A further study using R6G as the resonant adsorbate demonstrates that the LSPR is extremely sensitive to environmental change and that it can detect the adsorbate's electronic structure changes caused by aggregation. This allows for studying of the electronic interaction of resonant molecules and metal nanoparticles and could improve the understanding of surface-enhanced spectroscopies.

The tunability of LSPR has been successfully explored as a signal transduction mechanism for the detection of electronic structure changes in resonant proteins that are caused by substrate molecule binding. Amplified spectral response to substrate binding is achieved when the LSPR of the silver nanosensor is optimized to be close to the molecular resonance of the protein, which originates from a strong coupling between the molecular resonance and the intrinsic LSPR of the nanoparticles. It is foreseeable that this discovery will provide guidance to the design and optimization of refractive-index-based sensing for biological targets with resonant chromophores.

With regard to single-nanoparticle spectroscopy, the effect on the LSPR spectrum of a single nanocube due to the presence of a dielectric substrate was discussed. A second dipolar LSPR peak

was observed, and this was attributed to the nanocube's asymmetric dielectric environment. This phenomenon was made possible by the unique structure of a nanocube; it is thicker than the silver skin depth and has sharp corners that serve to concentrate the enhanced near fields induced by the LSPR.

Inhomogeneous and homogeneous linewidth broadening were discussed within the context of single silver triangular nanoprisms. It was found that the degree of tip sharpness in these structures is the dominant factor in determining the LSPR linewidth. This result illuminated the complex situation that can arrive when attempting to optimize a nanoparticle sensor for a specific application. In the case discussed, there exists a trade-off between the magnitude of the LSPR shift that is larger for particles with sharper tips, and resolution of small shifts that is higher for particles with blunt features. A weighted FOM was discussed as a means to assess a nanoparticle's sensing performance for any geometry and adsorbate thickness.

The findings in this research open up the possibility to lower the limit of detection for existing LSPR sensors as well as designing novel LSPR biosensors. Single nanoparticles have been demonstrated as promising sensing platforms. In combination with the resonant adsorbate amplification mechanism, it is possible to achieve extremely sensitive single-nanoparticle LSPR sensors. Single nanoparticles are ideal for this type of investigation due to the geometric heterogeneity of ensemble nanoparticle suspensions. This allows one to "tune" to different LSPR energies by simply interrogating different individual nanoparticles on a single substrate. The effect of molecular resonances on the LSPR wavelength and lineshape can be combined with choice of nanoparticle size and shape to optimize sensor performance for different biological systems.

## REFERENCES


[1] U. Kreibig and M. Vollmer, *Cluster Materials,* vol. 25. Heidelberg, Germany: Springer-Verlag, 1995.

[2] G. C. Schatz, M. A. Young, and R. P. Van Duyne, "Electromagnetic mechanism of SERS," *Topics Appl. Phys.*, vol. 103, pp. 19–46, 2006.

[3] G. C. Schatz and R. P. Van Duyne, "Electromagnetic mechanism of surface-enhanced spectroscopy," in *Handbook of Vibrational Spectroscopy,* vol. 1, J. M. Chalmers and P. R. Griffiths, Eds. New York: Wiley, 2002, pp. 759–774.

[4] S. A. Maier, M. L. Brongersma, P. G. Kik, S. Meltzer, A. A. G. Requicha, B. E. Koel, and H. A. Atwater, "Plasmonics—A route to nanoscale optical devices (vol 13, pg 1501, 2001)," *Adv. Mater.*, vol. 15, pp. 562–562, Apr. 17, 2003.

[5] S. A. Maier, P. G. Kik, H. A. Atwater, S. Meltzer, E. Harel, B. E. Koel, and A. A. G. Requicha, "Local detection of electromagnetic energy transport below the diffraction limit in metal nanoparticle plasmon waveguides," *Nat. Mater.*, vol. 2, pp. 229–232, Apr. 2003.

[6] I. I. Smolyaninov, Y.-J. Hung, and C. C. Davis, "Surface plasmon dielectric waveguides," *Appl. Phys. Lett.*, vol. 87, pp. 241106-1–241106-3, 2005.

[7] J. R. Krenn, "Nanoparticle waveguides. Watching energy transfer," *Nat. Mater.*, vol. 2, pp. 210–211, 2003.

[8] W. L. Barnes, A. Dereux, and T. W. Ebbesen, "Surface plasmon subwavelength optics," *Nature*, vol. 424, pp. 824–830, Aug. 14, 2003.

[9] E. Ozbay, "Plasmonics: Merging photonics and electronics at nanoscale dimensions," *Science*, vol. 311, pp. 189–193, 2006.

[10] J. O. Vasseur, A. Akjouj, L. Dobrzynski, B. Djafari-Rouhani, and E. H. El Boudouti, "Photon, electron, magnon, phonon and plasmon mono-mode circuits," *Surf. Sci. Rep.*, vol. 54, pp. 1–156, 2004.

[11] H. J. Lezec, A. Degiron, E. Devaux, R. A. Linke, L. Martin-Moreno, F. J. Garcia-Vidal, and T. W. Ebbesen, "Beaming light from a subwavelength aperture," *Science*, vol. 297, pp. 820–822, Aug. 2, 2002.

[12] B. Pettinger, B. Ren, G. Picardi, R. Schuster, and G. Ertl, "Nanoscale probing of adsorbed species by tip-enhanced Raman spectroscopy," *Phys. Rev. Lett.*, vol. 92, pp. 196101–196104, Mar. 5, 2004.

[13] A. D. McFarland and R. P. Van Duyne, "Single silver nanoparticles as real-time optical sensors with zeptomole sensitivity," *Nano Lett.*, vol. 3, pp. 1057–1062, 2003.

[14] X. Y. Zhang, J. Zhao, A. V. Whitney, J. W. Elam, and R. P. Van Duyne, "Ultrastable substrates for surface-enhanced Raman spectroscopy: $Al_2O_3$ overlayers fabricated by atomic layer deposition yield improved anthrax biomarker detection," *J. Am. Chem. Soc.*, vol. 128, pp. 10304–10309, Aug. 9, 2006.

[15] A. D. McFarland, M. A. Young, J. A. Dieringer, and R. P. Van Duyne, "Wavelength-scanned surface-enhanced raman excitation spectroscopy," *J. Phys. Chem. B*, vol. 109, pp. 11279–11285, 2005.

[16] A. J. Haes, L. Chang, W. L. Klein, and R. P. Van Duyne, "Detection of a biomarker for alzheimer's disease from synthetic and clinical samples using a nanoscale optical biosensor," *J. Am. Chem. Soc.*, vol. 127, pp. 2264–2271, 2005.

[17] J. Zhao, X. Y. Zhang, C. R. Yonzon, A. J. Haes, and R. P. Van Duyne, "Localized surface plasmon resonance biosensors," *Nanomedicine*, vol. 1, pp. 219–228, 2006.

[18] J. M. Brockman, B. P. Nelson, and R. M. Corn, "Surface plasmon resonance imaging measurements of ultrathin organic films," *Annu. Rev. Phys. Chem.*, vol. 51, pp. 41–63, 2000.

[19] S. Link, Z. L. Wang, and M. A. El-Sayed, "Alloy formation of gold–silver nanoparticles and the dependence of the plasmon absorption on their composition," *J. Phys. Chem. B*, vol. 103, pp. 3529–3533, 1999.

[20] G. H. Chan, J. Zhao, E. M. Hicks, G. C. Schatz, and R. P. Van Duyne, "Plasmonic properties of copper nanoparticles fabricated by nanosphere lithography," *Nano Lett.*, vol. 7, pp. 1947–1952, 2007.

[21] C. L. Haynes and R. P. Van Duyne, "Nanosphere lithography: A versatile nanofabrication tool for studies of size-dependent nanoparticle optics," *J. Phys. Chem. B*, vol. 105, pp. 5599–5611, 2001.

[22] K. L. Kelly, E. Coronado, L. L. Zhao, and G. C. Schatz, "The optical properties of metal nanoparticles: The influence of size, shape, and dielectric environment," *J. Phys. Chem. B*, vol. 107, pp. 668–677, 2003.

[23] R. Jin, Y. C. Cao, E. Hao, G. S. Metraux, G. C. Schatz, and C. A. Mirkin, "Controlling anisotropic nanoparticle growth through plasmon excitation," *Nature*, vol. 425, pp. 487–490, 2003.

[24] T. R. Jensen, M. D. Malinsky, C. L. Haynes, and R. P. van Duyne, "Nanosphere lithography: Tunable localized surface plasmon resonance spectra of silver nanoparticles," *J. Phys. Chem. B*, vol. 104, pp. 10 549–10 556, 2000.

[25] L. J. Sherry, S.-H. Chang, G. C. Schatz, R. P. Van Duyne, B. J. Wiley, and Y. Xia, "Localized surface plasmon resonance spectroscopy of single silver nanocubes," *Nano Lett.*, vol. 5, pp. 2034–2038, 2005.

[26] M. D. Malinsky, K. L. Kelly, G. C. Schatz, and R. P. Van Duyne, "Chain length dependence and sensing capabilities of the localized surface plasmon resonance of silver nanoparticles chemically modified with alkanethiol self-assembled monolayers," *J. Am. Chem. Soc.*, vol. 123, pp. 1471–1482, 2001.

[27] G. Xu, Y. Chen, M. Tazawa, and P. Jin, "Surface plasmon resonance of silver nanoparticles on vanadium dioxide," *J. Phys. Chem. B*, vol. 110, pp. 2051–2056, 2006.

[28] A. Pinchuk, A. Hilger, G. von Plessen, and U. Kreibig, "Substrate effect on the optical response of silver nanoparticles," *Nanotechnology*, vol. 15, pp. 1890–1896, 2004.

[29] W. Huang, W. Qian, and M. A. El-Sayed, "The optically detected coherent lattice oscillations in silver and gold monolayer periodic nanoprism arrays: The effect of interparticle coupling," *J. Phys. Chem. B*, vol. 109, pp. 18881–18888, 2005.

[30] L. Zhao, K. L. Kelly, and G. C. Schatz, "The extinction spectra of silver nanoparticle arrays: influence of array structure on plasmon resonance wavelength and width," *J. Phys. Chem. B*, vol. 107, pp. 7343–7350, 2003.

[31] C. L. Haynes, A. D. McFarland, L. Zhao, R. P. Van Duyne, G. C. Schatz, L. Gunnarsson, J. Prikulis, B. Kasemo, and M. Kaell, "Nanoparticle optics: The importance of radiative dipole coupling in two-dimensional nanoparticle arrays," *J. Phys. Chem. B*, vol. 107, pp. 7337–7342, 2003.

[32] L. Gunnarsson, T. Rindzevicius, J. Prikulis, B. Kasemo, M. Kaell, S. Zou, and G. C. Schatz, "Confined plasmons in nanofabricated single silver particle pairs: Experimental observations of strong interparticle interactions," *J. Phys. Chem. B*, vol. 109, pp. 1079–1087, 2005.

[33] R. Yonzon Chanda, E. Jeoung, S. Zou, C. Schatz George, M. Mrksich, and P. Van Duyne Richard, "A comparative analysis of localized and propagating surface plasmon resonance sensors: The binding of concanavalin A to a monosaccharide functionalized self-sssembled monolayer," *J. Am. Chem. Soc.*, vol. 126, pp. 12 669–12 676, 2004.

[34] L. J. Sherry, R. Jin, C. A. Mirkin, G. C. Schatz, and R. P. Van Duyne, "Localized surface plasmon resonance spectroscopy of single silver triangular nanoprisms," *Nano Lett.*, vol. 6, pp. 2060–2065, 2006.

[35] B. J. Wiley, S. H. Im, Z.-Y. Li, J. McLellan, A. Siekkinen, and Y. Xia, "Maneuvering the surface plasmon resonance of silver nanostructures through shape-controlled synthesis," *J. Phys. Chem. B*, vol. 110, pp. 15 666–15 675, 2006.

[36] B. J. Wiley, Y. Xiong, Z.-Y. Li, Y. Yin, and Y. Xia, "Right bipyramids of silver: A new shape derived from single twinned seeds," *Nano Lett.*, vol. 6, pp. 765–768, 2006.

[37] C. L. Nehl, H. Liao, and J. H. Hafner, "Optical properties of star-shaped gold nanoparticles," *Nano Lett.*, vol. 6, pp. 683–688, 2006.

[38] R. Jin, Y. Cao, C. A. Mirkin, K. L. Kelly, G. C. Schatz, and J. G. Zheng, "Photoinduced conversion of silver nanospheres to nanoprisms," *Science*, vol. 294, pp. 1901–1903, 2001.

[39] J. Zhao, L. Jensen, J. Sung, S. Zou, G. C. Schatz, and R. P. Van Duyne, "Interaction of plasmon and molecular resonances for rhodamine 6G adsorbed on silver nanoparticles," *J. Am. Chem. Soc.*, vol. 129, pp. 7647–7656, 2007.

[40] A. J. Haes, S. Zou, J. Zhao, G. C. Schatz, and R. P. Van Duyne, "Localized surface plasmon resonance spectroscopy near molecular resonances," *J. Am. Chem. Soc.*, vol. 128, pp. 10 905–10 914, 2006.

[41] J. Zhao, A. Das, X. Zhang, G. C. Schatz, S. G. Sligar, and R. P. Van Duyne, "Resonance surface plasmon spectroscopy: Low molecular weight substrate binding to cytochrome P450," *J. Am. Chem. Soc.*, vol. 128, pp. 11 004–11 005, 2006.

[42] M. Gratzel, "Photoelectrochemical cells," *Nature*, vol. 414, pp. 338–344, Nov. 15, 2001.

[43] M. Gratzel, "Dye-sensitized solid-state heterojunction solar cells," *MRS Bull.*, vol. 30, pp. 23–27, Jan. 2005.

[44] A. B. F. Martinson, J. E. McGarrah, M. O. K. Parpia, and J. T. Hupp, "Dynamics of charge transport and recombination in ZnO nanorod array dye-sensitized solar cells," *Phys. Chem. Chem. Phys.*, vol. 8, pp. 4655–4659, 2006.

[45] S. Nie and S. R. Emory, "Probing single molecules and single nanoparticles by surface-enhanced Raman scattering," *Science*, vol. 275, pp. 1102–1106, 1997.

[46] A. M. Michaels, M. Nirmal, and L. E. Brus, "Surface enhanced Raman spectroscopy of individual rhodamine 6G molecules on large Ag nanocrystals," *J. Am. Chem. Soc.*, vol. 121, pp. 9932–9939, Nov. 3, 1999.

[47] Y. R. Leroux, J. C. Lacroix, K. I. Chane-Ching, C. Fave, N. Felidj, G. Levi, J. Aubard, J. R. Krenn, and A. Hohenau, "Conducting polymer electrochemical switching as an easy means for designing active plasmonic devices," *J. Am. Chem. Soc.*, vol. 127, pp. 16 022–16 023, Nov. 23, 2005.

[48] G. A. Wurtz, P. R. Evans, W. Hendren, R. Atkinson, W. Dickson, R. J. Pollard, A. V. Zayats, W. Harrison, and C. Bower, "Molecular plasmonics with tunable exciton-plasmon coupling strength in J-aggregate hybridized Au nanorod assemblies," *Nano Lett.*, vol. 7, pp. 1297–1303, May 2007.

[49] A. G. Montalban, S. J. Lange, L. S. Beall, N. S. Mani, D. J. Williams, A. J. P. White, A. G. M. Barrett, and B. M. Hoffman, "Seco-porphyrazines: Synthetic, structural, and spectroscopic investigations," *J. Org. Chem.*, vol. 62, pp. 9284–9289, 1997.

[50] M. Gouterman, "Optical spectra and electronic structure of porphyrins and related rings," *Porphyrins*, vol. 3, pp. 1–165, 1978.

[51] R. P. Linstead and M. Whalley, "Conjugated macrocycles. XXII. Tetraazaporphine(porphyrazine) and its metallic derivatives," *J. Chem. Soc.*, pp. 4839–4846, 1952.

[52] C. S. Velazquez, G. A. Fox, W. E. Broderick, K. A. Andersen, O. P. Anderson, A. G. M. Barrett, and B. M. Hoffman, "Star-porphyrazines: Synthetic, structural, and spectral investigation of complexes of the polynucleating porphyrazineoctathiolato ligand," *J. Am. Chem. Soc.*, vol. 114, pp. 7416–7424, 1992.

[53] A. J. Haes, S. Zou, G. C. Schatz, and R. P. Van Duyne, "A nanoscale optical biosensor: The long range distance dependence of the localized surface plasmon resonance of noble metal nanoparticles," *J. Phys. Chem. B*, vol. 108, pp. 109–116, 2004.

[54] A. J. Haes and R. P. Van Duyne, "A nanoscale optical biosensor: Sensitivity and selectivity of an approach based on the localized surface plasmon resonance spectroscopy of triangular silver nanoparticles," *J. Am. Chem. Soc.*, vol. 124, pp. 10 596–10 604, 2002.

[55] J. C. Riboh, A. J. Haes, A. D. McFarland, C. R. Yonzon, and R. P. Van Duyne, "A nanoscale optical biosensor: Real-time immunoassay in physiological buffer enabled by improved nanoparticle adhesion," *J. Phys. Chem. B*, vol. 107, pp. 1772–1780, 2003.

[56] L. S. Jung, C. T. Campbell, T. M. Chinowsky, M. N. Mar, and S. S. Yee, "Quantitative interpretation of the response of surface plasmon resonance sensors to adsorbed films," *Langmuir*, vol. 14, pp. 5636–5648, 1998.

[57] A. J. Haes, S. Zou, G. C. Schatz, and R. P. Van Duyne, "Nanoscale optical biosensor: Short range distance dependence of the localized surface plasmon resonance of noble metal nanoparticles," *J. Phys. Chem. B*, vol. 108, pp. 6961–6968, 2004.

[58] R. D. L. Kronig and H. A. Kramers, "Theory of absorption and dispersion in X-ray spectra," *Z. Phys.*, vol. 48, pp. 174–179, 1928.

[59] B. F. Draine, J., "Discrete-dipole approximation for scattering calculations," *J. Opt. Soc. Am. A*, vol. 11, pp. 1491–1499, 1994.

[60] D. W. Lynch and W. R. Hunter, in *Handbook of Optical Constants of Solids*, E. D. Palik, Ed. New York: Academic, 1985, pp. 350–356.

[61] S. A. Soper, H. L. Nutter, R. A. Keller, L. M. Davis, and E. B. Shera, "The photophysical constants of several fluorescent dyes pertaining to ultrasensitive fluorescence spectroscopy," *Photochem. Photobiol.*, vol. 57, pp. 972–977, Jun. 1993.

[62] P. Hildebrandt and M. Stockburger, "Surface-enhanced resonance raman-spectroscopy of rhodamine-6G adsorbed on colloidal silver," *J. Phys. Chem.*, vol. 88, pp. 5935–5944, 1984.

[63] V. M. Martinez, F. L. Arbeloa, J. B. Prieto, and I. L. Arbeloa, "Characterization of rhodamine 6G aggregates intercalated in solid thin films of laponite clay. 2— Fluorescence spectroscopy," *J. Phys. Chem. B*, vol. 109, pp. 7443–7450, Apr. 21, 2005.

[64] V. M. Martinez, F. L. Arbeloa, J. B. Prieto, T. A. Lopez, and I. L. Arbeloa, "Characterization of Rhodamine 6G aggregates intercalated in solid thin films of Laponite clay. 1. Absorption spectroscopy," *J. Phys. Chem. B*, vol. 108, pp. 20 030–20 037, Dec. 30, 2004.

[65] V. M. Martinez, F. U. Arbeloa, J. B. Prieto, T. A. Lopez, and I. L. Arbeloa, "Characterization of supported solid thin films of laponite clay. Intercalation of rhodamine 6G laser dye," *Langmuir*, vol. 20, pp. 5709–5717, Jul. 6, 2004.

[66] M. A. Noginov, M. Vondrova, S. M. Williams, M. Bahoura, V. I. Gavrilenko, S. M. Black, V. P. Drachev, V. M. Shalaev, and A. Sykes, "Spectroscopic studies of liquid solutions of R6G laser dye and Ag nanoparticle aggregates," *J. Opt. a-Pure Appl. Opt.*, vol. 7, pp. S219–S229, Feb. 2005.

[67] S. Dare-Doyen, D. Doizi, P. Guilbaud, F. Djedaini-Pilard, B. Perly, and P. Millie, "Dimerization of xanthene dyes in water: Experimental studies and molecular dynamic simulations," *J. Phys. Chem. B*, vol. 107, pp. 13 803–13 812, Dec. 18, 2003.

[68] R. Reisfeld, R. Zusman, Y. Cohen, and M. Eyal, "The spectroscopic behavior of rhodamine 6G in polar and non-polar solvents and in thin glass and pmma films," *Chem. Phys. Lett.*, vol. 147, pp. 142–147, Jul. 3, 1988.

[69] M. Kasha, "Energy transfer mechanisms and the molecular exciton model for molecular aggregates," *Radiat. Res.*, vol. 20, pp. 55–70, 1963.

[70] M. Kasha, H. R. Rawls, and M. A. El-Bayoumi, "Exciton model in molecular spectroscopy," *Pure Appl. Chem.*, vol. 11, pp. 371–392, 1965.

[71] G. Mie, "Contributions to the optics of turbid media, especially colloidal metal solutions," *Ann. Physik* (Weinheim, Germany), vol. 25, pp. 377–445, 1908.

[72] C. F. B. A. D. R. Huffman, *Absorption and Scattering of Light by Small Particles*. New York: Wiley, 1983.

[73] J. D. Lipscomb and I. C. Gunsalus, "Structural aspects of active-site of cytochrome P-450Cam," *Drug Metab. Dispos.*, vol. 1, pp. 1–5, 1973.

[74] S. G. Sligar, "Coupling of spin, substrate, and redox equilibria in cytochrome P450," *Biochemistry*, vol. 15, pp. 5399–5406, 1976.

[75] J. J. Mock, M. Barbic, D. R. Smith, D. A. Schultz, and S. Schultz, "Shape effects in plasmon resonance of individual colloidal silver nanoparticles," *J. Chem. Phys.*, vol. 116, pp. 6755–6759, 2002.

[76] C. L. Nehl, H. Liao, and J. H. Hafner, "Plasmon resonant molecular sensing with single gold nanostars," *Proc. SPIE-Int. Soc. Opt. Eng.*, vol. 6323, pp. 63230G-1–63230G-8, 2006.

[77] A. Kumar and S. Mital, "Synthesis and photophysics of purine-capped Q-CdS nanocrystallites," *Photochem. Photobiol. Sci.*, vol. 1, pp. 737–741, 2002.

[78] H. Liu, "Theoretical and experimental study on the electronic structure of clusters," *Wuhan Gongye Daxue Xuebao*, vol. 15, pp. 138–145, 1993.

[79] S.-H. Chang, S. K. Gray, and G. C. Schatz, "Surface plasmon generation and light transmission by isolated nanoholes and arrays of nanoholes in thin metal films," *Opt. Exp.*, vol. 13, pp. 3150–3165, 2005.

[80] A. J. Haes, J. Zhao, S. Zou, C. S. Own, L. D. Marks, G. C. Schatz, and R. P. Van Duyne, "Solution-phase, triangular Ag nanotriangles fabricated by nanosphere lithography," *J. Phys. Chem. B*, vol. 109, pp. 11 158–11 162, 2005.
[81] C. L. Haynes and R. P. Van Duyne, "Plasmon-sampled surface-enhanced raman excitation spectroscopy," *J. Phys. Chem. B*, vol. 107, pp. 7426–7433, 2003.
[82] U. Kreibig and M. Vollmer, *Optical Properties of Metal Clusters,* vol. 25. Heidelberg, Germany: Springer-Verlag, 1995.
[83] S. E.-S. Link and M. A. El-Sayed, "Spectral properties and relaxation dynamics of surface plasmon electronic oscillations in gold and silver nanodots and nanorods," *J. Phys. Chem. B*, vol. 103, pp. 8410–8426, 1999.
[84] A. J. Haes, S. Zou, G. C. Schatz, and R. P. Van Duyne, "A nanoscale optical biosensor: The long range distance dependence of the localized surface plasmon resonance of noble metal nanoparticles," *J. Phys. Chem. B*, vol. 108, pp. 109–116, 2004.
[85] A. V. Whitney, J. W. Elam, S. Zou, A. V. Zinovev, P. C. Stair, G. C. Schatz, and R. P. Van Duyne, "Localized surface plasmon resonance nanosensor: A high-resolution distance-dependence study using atomic layer deposition," *J. Phys. Chem. B*, vol. 109, pp. 20 522–20 528, 2005.
[86] F. Tam, C. Moran, and N. Halas, "Geometrical parameters controlling sensitivity of nanoshell plasmon resonances to changes in dielectric environment," *J. Phys. Chem. B*, vol. 108, pp. 17 290–17 294, Nov. 11, 2004.
[87] F. Kim, J. H. Song, and P. D. Yang, "Photochemical synthesis of gold nanorods," *J. Am. Chem. Soc.*, vol. 124, pp. 14 316–14 317, Dec. 4, 2002.

**Jing Zhao** received the B.S. degree in chemical physics from the University of Science and Technology of China, Hefei, Anhui, China, in 2003. Currently, she is working toward the Doctoral degree in the Department of Chemistry, Northwestern University, Evanston, IL, where she is also a graduate student jointly between Prof. Richard P. Van Duyne's and Prof. George C. Schatz's groups.

Her current research interests include experimental and theoretical studies of the mechanisms and applications of localized surface plasmon resonance and surface-enhanced Raman spectroscopy.

Ms. Zhao was the recipient of the MRS Graduate Student Silver Award, The International Society for Optical Engineers (SPIE) Scholarship, the Phi Lambda Upsilon Gelewitz Award, and the Outstanding Researcher Award from Northwestern Nanoscale Science and Engineering Center (NSEC) in 2007.

**Leif J. Sherry** received the Undergraduate degree in chemistry from Centenary College of Louisiana, Shreveport, in 2002, and the Ph.D. degree in chemistry from Northwestern University, Evanston, IL, in 2007, under the direction of Prof. Richard P. Van Duyne and Prof. George Schatz.

He is currently with the Center for Naval Analyses, Washington, DC. His current research interests include experimental and theoretical studies of single-nanoparticle localized surface plasmon resonances.

Dr. Sherry was the recipient of the Outstanding Researcher Award from Northwestern Nanoscale Science and Engineering Center (NSEC) in 2006.

**George C. Schatz** received the Ph.D. degree from California Institute of Technology Research, Los Angeles, in 1976.

He is currently the Morrison Professor of Chemistry at Northwestern University, Evanston, IL. His current research interests include using theory and computation to describe physical phenomena in a broad range of applications relevant to chemistry, physics, biology, and engineering. The applications include optical properties of nanoparticles and nanoparticle assemblies; using theory to model polymer properties; DNA structure, thermodynamics, and dynamics; modeling self-assembly and nanopatterning; and gas-phase reaction dynamics.

Prof. Schatz was a Fellow of the American Physical Society in 1987 and the American Association for the Advancement of Science in 1999. He was elected to the International Academy of Quantum Molecular Sciences in 2001, to the American Academy of Arts and Sciences in 2002, and to the National Academy of Sciences in 2005. He was the recipient of numerous awards including the National Science Foundation Fellowship during 1971–1974, the Herbert Newby McCoy Award in 1975, the Northwestern Faculty Honor Roll in 1978–1979, the Alfred P. Sloan Research Fellow in 1980–1982, the Camille and Henry Dreyfus Teacher-Scholar in 1981–1986, the Fresenius Award (of Phi Lambda Upsilon) in 1983, the Japan Society for Promotion of Science Fellowship in 1986, and the Max Planck Research Award in 1993.

**Richard P. Van Duyne** received the Ph.D. degree from the University of North Carolina at Chapel Hill, Chapel Hill.

He is currently the Charles E. and Emma H. Morrison Professor of Chemistry at Northwestern University, Evanston, IL. His current research interests include surface-enhanced spectroscopy for chemical and biological sensing, nanofabrication, nanoparticle optics, scanning probe microscopy, Raman microscopy, Raman spectroscopy of mass-selected clusters, ultrahigh vacuun (UHV) surface science, and structure and function of biomolecules on surfaces.

Prof. Van Duyne was a member of the American Academy of Arts and Sciences in 2004, a Fellow of the American Physical Society in 1985, and a Fellow of the American Association for the Advancement of Science in 1983. He was the recipient of several awards including the L'Oreal Art and Science of Color Prize in 2006, the Nobel Laureate Signature Award for Graduate Education in Chemistry, the American Chemical Society Award in 2005, the Earle K. Plyler Prize for Molecular Spectroscopy from the American Physical Society in 2004, the Excellence in Surface Science Award of the Surfaces in Biomaterials Foundation in 1996, the Pittsburgh Spectroscopy Award in 1991, the Fresenius Award of Phi Lambda Upsilon in 1981, the Coblentz Memorial Prize in Molecular Spectroscopy in 1980, and the Alfred P. Sloan Fellowship in 1974–1978.